The Effect of Surfactants on Expanding Free Surfaces

C. J. W. Breward [a,b,1] R. C. Darton [c] P. D. Howell [b]
J. R. Ockendon [d]

[a] *Department of Pathology, University of Sheffield, Sheffield S10 2RX*

[b] *School of Mathematical Sciences, University of Nottingham, Nottingham NG7 2RD*

[c] *Department of Engineering Science, University of Oxford, Oxford OX1 3PJ*

[d] *Mathematical Institute, University of Oxford, Oxford OX1 3LB*

Abstract

This paper develops a systematic theory for the flow observed in the so-called "overflowing cylinder" experiment. The basic phenomenon to be explained is the order of magnitude increase in the surface velocity of a slowly overflowing beaker of water that is caused by the addition of a small amount of soluble surfactant. We perform analyses of (*i*) an inviscid bulk flow in which diffusion is negligible, (*ii*) a hydrodynamic boundary layer in which viscous effects become important, (*iii*) a diffusive boundary layer where diffusion is significant, and by matching these together arrive at a coupled problem for the liquid velocity and surfactant concentration. Our model predicts a relation between surface velocity and surface concentration which is in good agreement with experiment. However a degeneracy in the boundary conditions leaves one free parameter which must be taken from experimental data. We suggest an investigation that may resolve this indeterminacy.

Key words: Mathematical Modelling; Surfactant; Hydrodynamics; Interface; Diffusion

1 Introduction and experimental evidence

This paper concerns an experiment which illustrates the dramatic effect that small concentrations of surfactant can have on certain free surface flows. The

[1] Fax +44 114 2780059; e-mail C.Breward@sheffield.ac.uk

apparatus, shown schematically in Figure 1, consists of an open vertical cylinder brimful of water, which overflows gently as a result of a weak, deeply submerged pump (see *e.g.* Manning-Benson (1998) for a more detailed description). The surprising observation is that the addition of a small volume concentration of a suitable soluble surfactant can increase the overflow velocity by a factor that may be as large as ten.

Figure 1 about here

In crude terms, this phenomenon seems to be easy to explain. The pump produces a weak stagnation point flow at the centre of the overflowing surface and hence a gradual acceleration of the free surface as it expands away from the centre. Now the dissolved surfactant is attracted preferentially to the surface where, in the absence of the pump, it would reside in a monolayer with uniform surface concentration. However, the free surface expansion results in a decrease of the surface concentration relative to its value at the central stagnation point, and hence in a traction which is sufficient to produce a rapid acceleration of the monolayer. The theoretical quantification of this mechanism is the main objective of this paper and this will be seen to depend crucially on the relative importance of mechanical, diffusional and surface adsorption effects.

Flow straighteners ensure an approximately uniform vertical flow at the base of the cylinder and, as described in Manning-Benson, Bain & Darton (1997), Manning-Benson, Parker, Bain & Penfold (1998), Manning-Benson, Bain, Darton, Sharpe, Eastoe & Reynolds (1998), anemometry, surface light scattering and ellipsometry are used to determine, non-invasively, the shape of the free surface, the surface tension, the surface concentration of surfactant and the surface and subsurface velocities. The measurements are confined to a region within around 2.5 cm of the axis of the cylinder, whose radius is 4 cm, and the principal results are that

(1) the free surface is indistinguishable from a horizontal plane;
(2) the radial surface velocity increases roughly linearly with distance from the centre as in Figure 2, the acceleration increasing with the bulk surfactant concentration;

Figure 2 about here

(3) the subsurface velocity decreases away from the free surface as shown in

Figure 3;

Figure 3 about here

(4) the surface surfactant concentration Γ decreases slightly with distance from the axis as in Figure 4;

Figure 4 about here

(5) the surface tension γ varies as in Figure 5, the general shape of these curves being in accord with those of Figure 2 (in the sense that, as the concentration of surfactant increases, the slope of the curves in Figure 2 increases and the surface tension at the centre decreases);

Figure 5 about here

(6) all the above results change imperceptibly when the cylinder radius is changed (radii of 3, 4 and 5 cm have been used), indicating that the flow is independent of the cylinder radius so long as it is sufficiently large. Similarly, changing the shape of the rim of the cylinder (by means of various flanges) does not affect the measurements on the surface;
(7) providing it is greater than a critical value (to ensure that the liquid overflows steadily), the pump velocity has negligible effect on the surface velocity.

These results are typical for a surfactant below its critical micelle concentration so that there is no kinetic barrier to adsorption at the surface. We thus have a plethora of results that are invaluable in modelling flows induced by the presence of surfactants. They give us the basis for the physical assumptions to be made in §§2–3 which lead to the mathematical model of §4, which is analysed and discussed in §§5–6.

2 Preliminary modelling

2.1 Physical assumptions

Previous theoretical work on the overflowing cylinder has been based on the assumption that the flow is mostly in a boundary layer near the surface, driven by a shear stress which is estimated *a priori* (see Bergink-Martens, Bos, Prins & Schulte (1990), Bergink-Martens, Bos, Prins & Zuidberg (1992), Bergink-Martens, Bos & Prins (1994), Grunnet-Jepsen, Darton & Whalley (1995)). In this paper we present a systematic theoretical development which should enable us to predict the graphs in Figures 2–5, and in particular the surface velocities and concentrations, just from a knowledge of the pump velocity U_p, the cylinder radius a and the physical and chemical properties of the surfactant solution. These include its density ρ, dynamic viscosity μ and the diffusion coefficient D, all of which are assumed to be constant. Thus our governing equations for the water velocity $\boldsymbol{u}$ and pressure p are the Navier-Stokes equations

$$\nabla \cdot \boldsymbol{u} = 0, \quad \rho\left(\frac{\partial \boldsymbol{u}}{\partial t} + \boldsymbol{u} \cdot \nabla \boldsymbol{u}\right) = -\nabla p + \mu \nabla^2 \boldsymbol{u}, \tag{1}$$

while the bulk surfactant concentration C satisfies the linear advection-diffusion equation

$$\frac{\partial C}{\partial t} + \boldsymbol{u} \cdot \nabla C = D \nabla^2 C. \tag{2}$$

The experiments are conducted under steady state conditions so that in (1), (2) and henceforth all time derivatives may be neglected. Moreover, the symmetry of the experimental setup suggests that the flow is axisymmetric. Thus we adopt cylindrical polar coordinates (r, z), with r measuring radial distance from the axis of the cylinder and the z-axis pointing vertically upwards from the top of the cylinder, as shown in Figure 1. We denote the velocity components in the r- and z-directions by u_r and u_z.

We can get some idea of the dominant mechanisms by calculating dimensionless parameters based on the pump velocity. We find the Reynolds number $\rho a U_p/\mu$ is of order 10^2, the Péclet number aU_p/D is of order 10^5, the Froude number $U_p/\sqrt{ga}$ is of order 10^{-3} and the capillary number $U_p\mu/\gamma_w$, based on the surface tension γ_w of pure water, is of order 10^{-4} (values for ρ, a, U_p, D, μ and γ_w are given later in §3). However, these estimates may all have to be multiplied by a factor of 10 to account for the observed ratio of surface to pump velocities when surfactant is added.

In any event, the fact that the Froude number is at most of order 10^{-3} explains the observed flatness of the free surface and motivates our taking the simplifying "infinite gravity" limit in which the free surface is perfectly flat.

Thus we henceforth locate the free surface at $z = 0$ and ignore the normal stress condition (which could be used to obtain the first-order surface elevation *a posteriori*). Then neither gravity nor capillarity plays any further role in the modelling, and of the free-surface stress condition only the tangential component remains, namely

$$\frac{\mathrm{d}\gamma}{\mathrm{d}r} = \mu \frac{\partial u_r}{\partial z} \quad \text{on} \quad z = 0. \tag{3}$$

This represents a balance between viscous traction and the "Marangoni" stress due to a gradient in the surface tension γ.

Next we impose conservation of surfactant at the free surface ($z = 0$) by relating changes in the surface concentration Γ to the flux of surfactant up from the bulk. Surface diffusion is neglected throughout, as will be justified *a posteriori* in §3. The resulting equation is

$$D \frac{\partial C}{\partial z} = -\frac{1}{r} \frac{\mathrm{d}}{\mathrm{d}r} \left(r U_s \Gamma \right) \quad \text{on} \quad z = 0, \tag{4}$$

where we introduce U_s as shorthand for the surface velocity:

$$U_s(r) = u_r(r, 0).$$

To close the problem two constitutive relations are required between the surface tension and the surface and bulk concentrations, and these can be obtained by considering the thermodynamics of the interface. Rates of molecular interchange there are assumed to be sufficiently rapid for thermodynamic equilibrium to exist between the surface concentration Γ and the subsurface bulk concentration defined as

$$C_s(r) = C(r, 0).$$

As discussed in Adamson (1982), this implies a functional relation between C_s and Γ, which for our purposes is adequately described by the Langmuir isotherm

$$\Gamma = \Gamma_{\mathrm{sat}} \frac{C_s}{k + C_s}. \tag{5}$$

Here Γ_{sat} is the largest concentration that the surface can sustain and k is a material property of the surfactant-solvent system under consideration (with the same units as C). Typical values for both parameters will be given in §3.

We also appeal to thermodynamic equilibrium under the assumed isothermal conditions to relate surface tension and surface concentration. As shown in Adamson (1982), this gives rise to the Frumkin equation,

$$\gamma - \gamma_w = RT\Gamma_{\mathrm{sat}} \log \left(1 - \frac{\Gamma}{\Gamma_{\mathrm{sat}}} \right), \tag{6}$$

where R is the gas constant, T is the absolute temperature and we recall that γ_w is the surface tension of pure water. Since only gradients in γ enter our model, its absolute value is irrelevant, and the relations

$$\frac{\mathrm{d}\gamma}{\mathrm{d}\Gamma} = -\frac{RT}{1-\Gamma/\Gamma_{\mathrm{sat}}}, \quad \frac{\mathrm{d}\gamma}{\mathrm{d}C_s} = -\frac{RT\Gamma_{\mathrm{sat}}}{k+C_s} \tag{7}$$

are of more interest.

The boundary conditions (3)–(7) lie at the heart of our model. They are supplemented by conventional boundary conditions at the cylinder edge $r = r_0$ and symmetry conditions on the axis $r = 0$. Finally, at the bottom of the cylinder we assume the solution is fed in as a uniform plug flow (at velocity U_p) with a prescribed concentration C_b of surfactant.

Before we can proceed to a dimensionless model, we need to make some quantitative estimates, and we do this in §3. At the moment the only physical assumptions we can make with confidence are the following:

(1) the free surface is flat to lowest order;
(2) since the Reynolds number is large, the flow is basically inviscid except in hydrodynamic boundary layers on the walls and at the free surface (as suggested by Figure 3);
(3) since the Péclet number is large, diffusion is negligible except in a diffusive boundary layer at the free surface.

2.2 A mathematical paradigm

The situation is so complicated mathematically that it is helpful to close this section with a dimensionless paradigm which reflects the theory that will emerge in §4. A principal aim of this is to get an idea of the boundary conditions that will lead to a well-posed mathematical problem, and for this reason it is useful to include time dependence.

Suppose we consider an evolving surface monolayer lying along the x-axis and, starting at $t = 0$, supply dissolved surfactant to it at a rate of unity. Thus if the monolayer has surface concentration $\Gamma(x,t)$ and speed $u(x,t)$, then mass conservation requires (*cf.* (4))

$$\frac{\partial\Gamma}{\partial t} + \frac{\partial}{\partial x}(u\Gamma) = 1. \tag{8a}$$

Now, by analogy with (6) assume that γ is related to Γ by $\gamma + \Gamma = \text{const}$, so that

$$\frac{\partial\gamma}{\partial x} = -\frac{\partial\Gamma}{\partial x}.$$

If there is a bulk flow $u_b(x)$ below the monolayer then the simplest possible analogue of (3) is

$$\frac{\partial \gamma}{\partial x} = u - u_b. \tag{8b}$$

Putting all this together, we find that Γ satisfies the inhomogeneous "porous medium equation"

$$\frac{\partial \Gamma}{\partial t} = \frac{\partial}{\partial x}\left(\Gamma\left(\frac{\partial \Gamma}{\partial x} - u_b\right)\right) + 1. \tag{8c}$$

The model (8c) gives us the helpful idea that Γ diffuses nonlinearly over the surface, and we expect corresponding initial and boundary conditions to be applied on Γ before we have a well-posed mathematical problem. We shall return to this paradigm in §5.

The porous medium equation has been derived previously by Jensen and Halpern (1998) for the flow of insoluble surfactant on the surface of a thin viscous film held flat by gravity, although there is no analogue of u_b or the source term in that situation.

3 Boundary Layer Estimates

Approximate physical data for the experiments under consideration are as follows:

$$\begin{aligned}
a &\approx 4 \times 10^{-2}\,\mathrm{m}, & U_p &\approx 0.003\,\mathrm{m\,s^{-1}},\\
\rho &\approx 10^{3}\,\mathrm{kg\,m^{-3}}, & \mu &\approx 10^{-3}\,\mathrm{kg\,m^{-1}\,s^{-1}},\\
C_b &\approx 0.5\,\mathrm{mol\,m^{-3}}, & k &\approx 0.08\,\mathrm{mol\,m^{-3}},\\
D &\approx 5 \times 10^{-10}\,\mathrm{m^2\,s^{-1}}, & \Gamma_{\mathrm{sat}} &\approx 4 \times 10^{-6}\,\mathrm{mol\,m^{-2}},\\
\gamma_w &\approx 7 \times 10^{-2}\,\mathrm{N\,m^{-1}}, & RT &\approx 2500\,\mathrm{J\,mol^{-1}}.
\end{aligned}$$

In particular, the material parameters k and Γ_{sat} are determined by fitting the Langmuir isotherm (5) with experimentally measured (static) values of Γ and C_s, as shown in Figure 6. It is clear that the best fit shown is not particularly good, so our predicted values of k and Γ_{sat} are probably not very accurate.

Figure 6 about here

We now consider the orders of magnitude of the terms in the model that are responsible for the existence of the boundary layers at the surface $z = 0$. For the moment we consider an arbitrary length-scale L for the radial distance r; a suitable choice of L will be made shortly. We recall that near the axis of the cylinder flow takes the form of a stagnation point, in which the radial velocity u_r increases linearly with r (see Figure 2). Thus it makes sense to characterise the flow by a typical dilatation rate α so that the order of magnitude for u_r is αL.

It turns out that the mass balance (4) gives the strongest clue to the size of α. Assuming, as evidenced by Figure 4, that C varies by $O(C_b)$ across the diffusional boundary layer and that $\Gamma/\Gamma_{\text{sat}} = O(1)$, we have

$$\frac{DC_b}{L\text{Pe}^{-1/2}} \sim \Gamma_{\text{sat}}\alpha, \tag{9}$$

where $L\text{Pe}^{-1/2}$ is the diffusive boundary layer thickness, with Péclet number $\text{Pe} = \alpha L^2/D$ based on the velocity scale αL. We can rearrange (9) to give an estimate for the dilatation rate α:

$$\alpha \sim \frac{DC_b^2}{\Gamma_{\text{sat}}^2} \sim 8\,\text{s}^{-1} \text{ when } C_b = 0.5\,\text{mol}\,\text{m}^{-3}. \tag{10}$$

This is in agreement with the experimental observation that the strength of the stagnation point flow is intrinsic, *i.e.* it depends on neither the pump velocity nor the cylinder radius. Furthermore, in order of magnitude, equation (10) is consistent with Figure 2, although the experimental evidence points to rather less sensitive dependence on C_b: (10) agrees well with Figure 2 at low concentrations, but overestimates α by a factor of about four when $C_b = 0.58\,\text{mol}\,\text{m}^{-3}$. The reason for this is that the variation of C across the diffusional boundary layer is significantly less than C_b at the higher concentrations, and this needs to be explained by our model.

Thus we proceed by using

$$\alpha = DC_b^2/\Gamma_{\text{sat}}^2 \tag{11}$$

as our estimate of the dilatation rate. In terms of this, the diffusion boundary layer has thickness

$$\sqrt{\frac{D}{\alpha}} = \frac{\Gamma_{\text{sat}}}{C_b}, \tag{12}$$

which corresponds physically to the thickness of the "catchment region" at bulk concentration C_b needed to replenish a surface concentration of Γ_{sat}, and is around $8\,\mu$m when $C_b = 0.5\,\text{mol}\,\text{m}^{-3}$.

Similarly we can define the thickness of the hydrodynamic boundary layer by $L\text{Re}^{-1/2}$ where Re is the Reynolds number based on the velocity scale αL.

Notice that the hydrodynamic boundary layer is thicker than the diffusive boundary layer by a factor of $1/\delta$ where

$$\delta^2 = \frac{\rho D}{\mu} \tag{13}$$

is the Prandtl number. Using the estimated parameter values given above, we obtain $\delta \approx 0.02$, and indeed under all physical conditions of interest δ is small. This will enable us partially to decouple the hydrodynamic and diffusive problems in §4.

The explanation for the dramatic increase in the surface velocity when the surfactant is added is now evident when we compare α with the strength of the stagnation point flow generated by the pump in the absence of any surfactant:

$$\frac{U_p}{a} \sim 0.08\,\mathrm{s}^{-1}.$$

Thus the ratio of the pump velocity to the surfactant-generated velocity

$$\frac{U_p}{\alpha a} = \frac{U_p \Gamma_{\mathrm{sat}}^2}{a D C_b^2} = \epsilon \tag{14}$$

is a small parameter, even if we use the experimentally measured values for α rather than the estimate (10).

The surface tension variations are estimated from the mechanical balance (3) as

$$\Delta\gamma \sim \frac{\mu\alpha L}{\mathrm{Re}^{-1/2}} \sim L^2\sqrt{\rho\mu\alpha^3}. \tag{15}$$

The quadratic dependence on the length-scale L ties in with our expectation that surface tension should vary quadratically near the stagnation point. We now use (7) to derive estimates for the corresponding radial variations in the surface and subsurface concentrations Γ and C_s

$$\Delta\Gamma \sim \frac{L^2\sqrt{\rho\mu\alpha^3}}{RT}, \quad \frac{\Delta C_s}{C_b} \sim \frac{L^2\sqrt{\rho\mu\alpha^3}}{\Gamma_{\mathrm{sat}} RT}, \tag{16}$$

which are in accordance with Figure 4.

It now emerges that an intrinsic length-scale L can be defined, over which C_s varies by an order one amount compared to C_b, namely

$$L = \frac{\sqrt{\Gamma_{\mathrm{sat}} RT}}{(\rho\mu\alpha^3)^{1/4}} = \frac{\Gamma_{\mathrm{sat}}^2\sqrt{RT}}{C_b^{3/2}\,(\rho\mu D^3)^{1/4}} \sim 20\,\mathrm{mm} \text{ when } C_b = 0.5\,\mathrm{mol\,m}^{-3}. \tag{17}$$

The significance of this L is that we should expect the surface concentration to be effectively constant only over radial distances smaller than $O(L)$.

We now have to make a judgement concerning the relative sizes of the length-scale L and the cylinder radius a, and to this end we define $r_0 = a/L$. At first glance L appears to be a fraction of the cylinder radius and roughly the same as a typical measurement radius, which suggests considering the regime $r_0 \gg 1$. However, recall that our expression for α is in general an overestimate, so that the length-scale over which C_s varies significantly is probably somewhat longer in practice; this explains why Γ appears to be virtually constant in Figure 4. Thus we treat r_0 as a constant of order one when we carry out an approximate analysis for small ϵ, *i.e.*,

$$r_0^2 = \frac{a^2}{L^2} = \frac{a^2\sqrt{\rho\mu\alpha^3}}{RT\Gamma_{\rm sat}} = \frac{a^2 C_b^3\sqrt{\rho\mu D^3}}{RT\Gamma_{\rm sat}^4} = O(1). \tag{18}$$

If our model were to be applied to experiments carried out with significantly wider cylinders, it might make sense to consider the limit $r \sim L$, $L \ll a$ (*i.e.* $r_0 \gg 1$). However, the results of such an analysis would be analogous to the expansions carried out in §5 assuming $r \ll L$, $L \sim a$ (*i.e.* $r_0 = O(1)$).

At this stage we can verify that we were justified in neglecting surface diffusion, whose importance may be determined by comparing diffusion with convection in the surface. The corresponding dimensionless parameter group is

$$\frac{D_s}{\alpha L} = \frac{D_s C_b\sqrt{\rho\mu D}}{\Gamma_{sat}^2 RT},$$

where, according to Jensen and Halpern (1998), the surface diffusion coefficient $D_s \leq 10^{-9}\,\mathrm{m^2\,s^{-1}}$ for typical surfactants. Thus $D_s/(\alpha L) \leq 10^{-6}$ and the effect of surface diffusion is indeed negligible.

We are now in a position to write down the mathematical model for the overflowing cylinder.

4 The Mathematical Model

4.1 Bulk Flow

Following the discussion in §3, we begin by nondimensionalising r and z with the distinguished length-scale L and the velocity $\boldsymbol{u} = (u_r, u_z)$ with αL, where α is as defined in (11). As pointed out in §2, the fluid dynamics of the bulk flow is approximately that of an irrotational, inviscid, radially symmetric flow in which a free stream impinges on the flat surface $z = 0$. Thus, if we define

a streamfunction $\psi(r,z)$ in the usual way such that

$$u_r(r,z) = \frac{1}{r}\frac{\partial \psi}{\partial z}, \quad u_z(r,z) = -\frac{1}{r}\frac{\partial \psi}{\partial r},$$

then, away from any boundary layers ψ satisfies

$$\frac{\partial^2 \psi}{\partial r^2} - \frac{1}{r}\frac{\partial \psi}{\partial r} + \frac{\partial^2 \psi}{\partial z^2} = 0. \tag{19}$$

When writing down the boundary conditions for (19), we are at liberty to choose ψ to be zero on the streamline travelling up the axis of the cylinder and along the free surface. We also model the effect of the flow straighteners by imposing a uniform plug flow as z approaches minus infinity, and thus we have

$$\psi = 0 \text{ on } z = 0, r < r_0, \tag{20a}$$

$$\psi \sim -\epsilon\frac{r^2}{2} \text{ as } z \to -\infty, r < r_0, \tag{20b}$$

$$\psi = 0 \text{ on } r = 0, z < 0, \tag{20c}$$

$$\psi = -\epsilon\frac{r_0^2}{2} \text{ on } r = r_0, z < 0, \tag{20d}$$

where we recall $r_0 = a/L = O(1)$ and $\epsilon = U_p/(\alpha L)$ is a small parameter. The solution to (19), (20) is

$$\psi = \frac{\epsilon r_0 r}{\pi}\int_0^\infty \frac{I_1(kr)\sin kz}{kI_1(kr_0)}dk, \tag{21}$$

where I_1 denotes a modified Bessel function.

Now we evaluate the radial velocity u_r on the free surface $z = 0$. We denote this by $\epsilon u_b(r)$: it is the "bulk velocity" which will be used for matching with the boundary layer on $z = 0$:

$$\begin{aligned}\frac{u_r(r,0)}{\epsilon} = u_b(r) &= \frac{r_0}{\pi}\int_0^\infty \frac{I_1(kr)}{I_1(kr_0)}dk \\ &\sim \begin{cases} 0.89\dfrac{r}{r_0} + 0.67\left(\dfrac{r}{r_0}\right)^3 + O\left(\dfrac{r}{r_0}\right)^5 & \text{as } r \to 0, \\ \dfrac{r_0}{\pi(r_0 - r)} + O(1) & \text{as } r \to r_0. \end{cases}\end{aligned} \tag{22}$$

In the limit as $z \to 0$, u_r differs from this function by $O(z^2)$, since the bulk flow is irrotational.

Note that, near the rim $r = r_0$, the bulk flow has the form of an inviscid sink at which fluid is removed at a rate which exactly balances the flux fed into the bottom of the cylinder. Our "infinite gravity" limit is responsible for the velocity being unbounded at the rim. In practice there is a small region resembling a two-dimensional "weir flow", whose size is determined by the Froude number (assumed zero in this paper). Equation (22) only applies outside this region. We do not attempt to model this complicated weir flow in this paper, but its possible implications for surfactant transport are discussed briefly in §5.3.

Concerning the surfactant concentration, as pointed out in §2, mass transfer by diffusion is negligible in the bulk. It follows that the concentration C, nondimensionalised with C_b, is simply given by

$$C \equiv 1, \tag{23}$$

to lowest order. However, this "outer solution" (21), (23) violates the free surface boundary conditions, and thus boundary layers must be introduced near $z = 0$. (There are also boundary layers near the edge of the cylinder $r = r_0$, but these are of less interest to us.)

4.2 Surface Boundary Layers

We have already commented that the hydrodynamic boundary layer which is needed to adjust the bulk flow to the traction condition (3) has thickness $L\mathrm{Re}^{-1/2}$, where $\mathrm{Re} = \rho\alpha L^2/\mu$. Thus we rescale

$$z = \mathrm{Re}^{-1/2} z_h, \quad u_z = \mathrm{Re}^{-1/2}\tilde{u}_z, \tag{24}$$

and the boundary layer model is then found to be

$$u_r \frac{\partial u_r}{\partial r} + \tilde{u}_z \frac{\partial u_r}{\partial z_h} = -\frac{\partial p}{\partial r} + \frac{\partial^2 u_r}{\partial z_h^2}, \tag{25a}$$

$$0 = \frac{\partial p}{\partial z_h}, \tag{25b}$$

$$\frac{1}{r}\frac{\partial}{\partial r}(r u_r) + \frac{\partial \tilde{u}_z}{\partial z_h} = 0, \tag{25c}$$

where pressure p is made dimensionless with $\rho\alpha^2 L^2$.

The obvious boundary and matching conditions are

$$u_r = 0 \ \text{ on } \ r = 0, \tag{26a}$$

$$\tilde{u}_z = 0 \ \text{ on } \ z_h = 0, \tag{26b}$$

and

$$u_r \to \epsilon u_b(r), \quad \tilde{u}_z \sim -\frac{\epsilon z_h}{r}\frac{\mathrm{d}}{\mathrm{d}r}\left(r u_b\right) \quad \text{as} \quad z_h \to -\infty, \tag{26c}$$

the smallness of ϵ reflecting the fact that the boundary layer flow is effectively driven by the surfactant-generated shear at $z = 0$ rather than by the bulk flow. To quantify this shear we must consider the coupled problem for the concentration of surfactant.

The diffusive boundary layer that is needed for the bulk concentration to adjust to its surface value C_s has thickness $L\mathrm{Pe}^{-1/2}$, where $\mathrm{Pe} = \alpha L^2/D$. As noted in §3, this is thinner than the hydrodynamic boundary layer by a factor of $\delta \ll 1$. To examine this region we therefore rescale again, setting

$$z_d = \frac{z_h}{\delta} = \mathrm{Pe}^{1/2} z. \tag{27}$$

Note that in this layer the velocity components can be approximated by

$$\begin{aligned} u_r(r, \delta z_d) &\sim U_s(r) + O(\delta), \\ \tilde{u}_z(r, \delta z_d) &\sim -\delta \frac{z_d}{r}\frac{\mathrm{d}}{\mathrm{d}r}\left[r U_s(r)\right] + O(\delta^2), \end{aligned}$$

where as before $U_s(r) = u_r(r, 0)$, and hence the concentration satisfies

$$\frac{\partial^2 C}{\partial z_d^2} = U_s(r)\frac{\partial C}{\partial r} - \frac{z_d}{r}\frac{\mathrm{d}}{\mathrm{d}r}\left[r U_s(r)\right]\frac{\partial C}{\partial z_d} \tag{28}$$

at leading order.

Again the obvious symmetry and matching conditions are

$$\frac{\partial C}{\partial r} = 0 \quad \text{on} \quad r = 0, \quad C \to 1 \quad \text{as} \quad z_d \to -\infty.$$

As before we define C_s to be the subsurface bulk concentration and use (5) to relate it to the surface concentration Γ (made dimensionless with Γ_{sat}):

$$C(r, 0) = C_s(r), \quad \Gamma = \frac{C_s(r)}{\beta + C_s(r)}, \tag{29}$$

where

$$\beta = \frac{k}{C_b}$$

is an order one dimensionless constant. Then our boundary condition (4), representing conservation of surfactant, becomes

$$\frac{\partial C}{\partial z_d} = -\frac{1}{r}\frac{\mathrm{d}}{\mathrm{d}r}\left(r U_s(r)\Gamma\right) \quad \text{on} \quad z_d = 0. \tag{30}$$

Finally we scale $d\gamma/dr$ using $\Delta\gamma/L$, where $\Delta\gamma$ is given in (15), to obtain the nondimensional form of (3) as

$$\frac{\mathrm{d}\gamma}{\mathrm{d}r} = \frac{\partial u_r}{\partial z_h}(r,0), \tag{31}$$

noting, of course, that $\partial u_r/\partial z_h$ does not change across the diffusion boundary layer. Here the surface tension gradient can be related to the concentration gradient using the dimensionless version of (7), namely

$$\frac{\mathrm{d}\gamma}{\mathrm{d}\Gamma} = -\frac{1}{1-\Gamma}, \quad \frac{\mathrm{d}\gamma}{\mathrm{d}C_s} = -\frac{1}{\beta + C_s}, \tag{32}$$

these being equivalent as a result of (29).

Equations (25)–(32) comprise our dimensionless model for u_r, $\tilde{u}_z$, C, Γ and γ. Notice that our choice of length- and velocity-scales has resulted in the constants of proportionality in (29)–(32) all being unity. The only remaining parameters are β and r_0, which are prescribed and $O(1)$, and ϵ which is also prescribed and which we will take to be small. The function $u_b(r)$ is likewise given *a priori* by (22), and provides the only coupling between the boundary layers and the outer flow.

We end this section by summarising the model equations and boundary conditions whose solution we will consider in the following section. As in §4.1 it is convenient to define a streamfunction, say $\tilde{\psi}$, such that

$$u_r = \frac{1}{r}\frac{\partial \tilde{\psi}}{\partial z_h}, \quad \tilde{u}_z = -\frac{1}{r}\frac{\partial \tilde{\psi}}{\partial r}.$$

In the interests of stating the model as simply as possible, we henceforth drop the tildes.

The field equations for the streamfunction and concentration are thus

$$\frac{\partial^3 \psi}{\partial z_h^3} = \frac{1}{r}\left[\frac{\partial \psi}{\partial z_h}\frac{\partial^2 \psi}{\partial r \partial z_h} - \frac{\partial \psi}{\partial r}\frac{\partial^2 \psi}{\partial z_h^2} - \frac{1}{r}\left(\frac{\partial \psi}{\partial z_h}\right)^2\right] - \epsilon^2 r u_b(r) u_b'(r), \tag{33}$$

$$\frac{\partial^2 C}{\partial z_d^2} = \frac{1}{r}\left[\frac{\partial \psi}{\partial z_h}(r,0)\frac{\partial C}{\partial r} - \frac{\partial^2 \psi}{\partial r \partial z_h}(r,0) z_d \frac{\partial C}{\partial z_d}\right], \tag{34}$$

with the symmetry and matching conditions

$$\psi = \frac{\partial C}{\partial r} = 0 \ \text{ on } \ r = 0, \tag{35}$$

$$\frac{\partial \psi}{\partial z_h} \to \epsilon r u_b(r), \quad C \to 1 \ \text{ as } \ z_d, z_h \to -\infty. \tag{36}$$

Now, using (29) and (32) we can state the boundary conditions on the free surface in terms only of ψ and C:

$$\psi = 0, \tag{37}$$

$$\frac{\partial C}{\partial z_d} = -\frac{1}{r}\frac{\partial}{\partial r}\left(\frac{C}{\beta + C}\frac{\partial \psi}{\partial z_h}\right), \tag{38}$$

$$\frac{1}{r}\frac{\partial^2 \psi}{\partial z_h^2} = -\frac{1}{\beta + C}\frac{\partial C}{\partial r}, \tag{39}$$

all to be applied on $z_h = z_d = 0$.

5 Solution of the Model

5.1 Local solution near the origin

The first step in our solution procedure is formally to set $\epsilon = 0$. Aside from the fact that the values given in §3 indicate that ϵ *is* reasonably small, we are further motivated by the experimental observation that the pump velocity has negligible influence on the flow generated at the surface. However, recall from (22) that the bulk flow u_b blows up as $r \to r_0$, so we should expect the limit $\epsilon \to 0$ to be nonuniform sufficiently close to the rim.

Even with ϵ set to zero the problem (33)–(39) is formidable. Indeed it is far from clear whether the boundary conditions given are sufficient to specify a unique solution. Therefore we begin by performing a coordinate expansion for small r, which corresponds to analysing the behaviour of the solution near the axis of the cylinder. There are several arguments for adopting this strategy, both physical and mathematical. First we recall that most of the experimental measurements have been made closer to the stagnation point than the rim. Moreover the insensitivity of these measurements to changes in the pump velocity and cylinder radius suggests that edge effects, which are ignored by our approach, have little influence on the local behaviour. Even if (as may turn out to be the case) this suggestion is ill-founded, a local analysis for small r will tell us the number of degrees of freedom for the solution near the origin, and thus give more information about the well-posedness of the model and suggest what further boundary conditions may need to be imposed.

Assuming that the concentration and velocity fields are analytic near the origin we can expand them as Taylor series as follows:

$$C(r, z_d) = \sum_{n=0}^{\infty} C_{2n}(z_d) r^{2n}, \quad \psi(r, z_h) = \sum_{n=0}^{\infty} f_{2n}(z_h) r^{2n+2}. \tag{40}$$

By substituting these expansions into (33)–(39) and equating coefficients of powers of r, we obtain a sequence of problems for the functions $f_0(z_h)$, $C_0(z_d)$, $f_2(z_h)$, $C_2(z_d)$ and so forth.

At leading order we have

$$f_0''' + 2f_0 f_0'' - (f_0')^2 = 0, \tag{41}$$
$$C_0'' + 2f_0'(0) z_d C_0' = 0, \tag{42}$$

$$f_0' \to 0 \ \text{ as } \ z_h \to -\infty, \tag{43}$$
$$C_0 \to 1 \ \text{ as } \ z_d \to -\infty, \tag{44}$$
$$f_0 = 0, \ \text{ on } \ z_h = 0, \tag{45}$$
$$C_0' = -\frac{2f_0' C_0}{\beta + C_0} \ \text{ on } \ z_h = z_d = 0. \tag{46}$$

The final boundary condition (39) yields

$$f_0'' = -\frac{2C_2}{\beta + C_0} \ \text{ on } \ z_h = z_d = 0, \tag{47}$$

which tells us nothing about the leading-order unknowns, but simply passes information on to the $O(r^2)$ problem for C_2.

Thus we appear to be missing one boundary condition for the leading-order problem: f_0 and C_0 are not determined uniquely by (41)–(46). There is a one-parameter family of solutions, which can be parametrised for example by $C_0(0)$. With $C_0(0)$ given, $C_0(z_d)$ is specified by (42), (44), in terms of the *a priori* unknown constant $f_0'(0)$, as

$$C_0(z_d) = 1 + (C_0(0) - 1)\,\mathrm{erfc}\left(-z_d\sqrt{f_0'(0)}\right). \tag{48}$$

Thus

$$C_0'(0) = 2\,(C_0(0) - 1)\sqrt{\frac{f_0'(0)}{\pi}},$$

and by substituting this into (46) we obtain an expression for $f_0'(0)$:

$$f_0'(0) = \frac{1}{\pi}\left(\frac{(\beta + C_0(0))(C_0(0) - 1)}{C_0(0)}\right)^2. \tag{49}$$

Now, for any given value of $C_0(0)$, (41), (43), (45), (49) *does* constitute a well-posed problem for $f_0(z_h)$, and indeed one which can readily be solved numerically. However, $C_0(0)$ corresponds to the subsurface concentration evaluated

at the origin, and as such should be a *prediction* of the model, rather than a parameter to be specified. Unfortunately there is no way in which a particular value of $C_0(0)$ can be selected within the leading-order equations (41)–(46).

Furthermore, this indeterminacy cannot be resolved simply by considering higher-order terms in the expansions (40). The $O(r^2)$ terms from (33)–(38), along with (47), give enough equations and boundary conditions to determine (in principle) the first corrections f_2 and C_2 *assuming* f_0 and C_0 are already known. The same holds at higher order: if all the f_{2k} and C_{2k} are known up to say $k = n - 1$, then the problem for f_{2n}, C_{2n} appears to be well-posed. Thus $C_0(0)$ remains as a free parameter which carries through every order of the expansions.

5.2 Comparison with experiments

Before embarking on a more thorough discussion of this apparent lack of uniqueness, we note that (49) leads us to a relationship between the strength of the stagnation point flow and the subsurface concentration at the stagnation point which, in dimensional form, reads

$$\frac{\mathrm{d}U_s}{\mathrm{d}r}(0) = \frac{D(C_b - C_s(0))^2(k + C_s(0))^2}{\pi\Gamma_{\mathrm{sat}}^2 C_s(0)^2}. \tag{50}$$

We also have, from the Langmuir isotherm (5),

$$\Gamma(0) = \Gamma_{\mathrm{sat}}\frac{C_s(0)}{k + C_s(0)}. \tag{51}$$

Thus, if both the bulk concentration C_b and the corresponding value of $\Gamma(0)$ are treated as data, we can read $C_s(0)$ from (51) and thus predict the dilatation rate $U_s'(0)$.

Figure 7 about here

To compare our theory with experiment we therefore start by plotting measurements of $\Gamma(0)$ versus C_b, as shown in Figure 7. Then, from (51), we deduce the corresponding values of the subsurface bulk concentration $C_s(0)$; it is worth noting that these values depend quite sensitively upon the Langmuir constants Γ_{sat} and k, which, as pointed out in §3, are not known with any accuracy. We can now use (50) to plot our prediction of $U_s'(0)$ versus C_b, shown as open circles in Figure 8. Note that the data point $\Gamma(0) = 0$ when $C_b = 0$ is not used

in Figure 8: the behaviour of $\Gamma(0)$ as $C_b \to 0$ is needed, and this cannot safely be deduced from the sparse data of Figure 7.

Figure 8 about here

The experimental values of $U_s'(0)$, obtained by fitting a cubic polynomial to the data in Figure 2 and reading off the linear term, are shown as closed circles. Despite the uncertainty about the correct values of Γ_{sat} and k, for bulk concentrations above $0.3\,\text{mol}\,\text{m}^{-3}$ the theory agrees reasonably well with the data, in both order of magnitude and trend. However, the predicted $U_s'(0)$ at $C_b = 0.1\,\text{mol}\,\text{m}^{-3}$ does not match that observed experimentally.

We have found that the theoretical value cannot be made to fit the data at the lower concentration by varying Γ_{sat} and k in line with the scatter of the points in Figure 6. Neither can the discrepancy be explained as a failure of the $\epsilon \to 0$ limit, although it is undoubtedly true that the Marangoni-induced surface velocity becomes the same order as the pump velocity at very low concentrations. The divergence between theory and experiment appears to begin at moderate values of C_b for which ϵ is still small and, in any case, it can be shown that the prediction (50) holds even if ϵ is order one.

The root of the problem appears to be the experimentally-measured behaviour of $\Gamma(0)$ shown in Figure 7. As the bulk concentration decreases, so does the surface dilatation rate, so we would expect the surface concentration to approach its static value, *i.e.* that shown in the Langmuir isotherm Figure 6. Figure 7, however, suggests that the surface concentration is consistently lower than its static value as $C_b \to 0$.

Clearly Figure 7 is based on only five data points and so should be treated with some caution, but anomalously low surface concentration has been observed previously at low bulk concentration, and attributed to an electric double layer caused by the accumulation of ionic surfactant molecules at the interface. Bain, Manning-Benson & Darton (2000) note that "mass transfer across the electric double layer is impeded by a potential barrier that becomes relatively more effective at low concentrations." Our model takes no account of any such barrier, which may explain its disagreement with the measurement taken at the lowest concentration.

5.3 Resolution of the indeterminacy

A clue to the origin of the lack of uniqueness in our solution comes from the paradigm introduced in §2.2. When we consider the steady state for that model and introduce a parameter ϵ analogous to that in (36), the paradigm becomes

$$\frac{\mathrm{d}}{\mathrm{d}x}(u\Gamma) = 1, \quad \frac{\mathrm{d}\gamma}{\mathrm{d}x} = u - \epsilon u_b(x), \quad \frac{\mathrm{d}\Gamma}{\mathrm{d}x} = -\frac{\mathrm{d}\gamma}{\mathrm{d}x}. \tag{52}$$

Thus, applying symmetry at $x = 0$ and assuming $u_b(0) = 0$, we have

$$\Gamma\left(\frac{\mathrm{d}\Gamma}{\mathrm{d}x} - \epsilon u_b(x)\right) = -x. \tag{53}$$

Evidently there is no way to determine $\Gamma(0)$ from (53) alone. However, if we formally set $\epsilon = 0$ as in §5.1, then the family of possible solutions is clearly parametrised by $\Gamma(0)$ as

$$\Gamma(x) = \sqrt{\Gamma(0)^2 - x^2}. \tag{54}$$

As is typical for such degenerate diffusion equations, Γ reaches zero at a finite value of x and, if (53) is to be solved on a finite region $0 \leq x < r_0$, then we must have $\Gamma(0) \geq r_0$.

Now, as pointed out in §5.1, if the bulk flow $u_b(x)$ has singular behaviour akin to (22) as $x \to r_0$, then, in the limit $\epsilon \to 0$, (54) breaks down near $x = r_0$. It is straightforward to perform an asymptotic analysis of (53) and thus to show that in general Γ blows up logarithmically as $x \to r_0$, there being exactly one value of $\Gamma(0)$ for which Γ remains bounded. Presumably *any* physically sensible boundary condition which might be applied on Γ at $x = r_0$ would force the solution to be finite and thus select the same value of $\Gamma(0)$. This agrees nicely with the observed insensitivity of the experiments to the conditions (*e.g.* wall thickness, shape, *etc.*) at the edge.

The selected value of $\Gamma(0)$ is

$$\Gamma(0) = r_0,$$

i.e. it is such that $\Gamma(r_0) = 0$. In our paradigm, the values of $\Gamma(0)$ depends on the "radius" r_0, in contrast with experiments. However we should keep in mind that (53) is a gross simplification of the full model, which we hope does not share this feature.

We are led by this simple paradigm, then, to suggest that some condition on Γ must be imposed at the rim of the cylinder to close our model, if only that Γ be bounded as $r \to r_0$. Even if this hypothesis is correct, our problem (33)–(39) is so much more complicated than (53) that the task of determining $\Gamma(0)$

uniquely is still very difficult mathematically. A possible future investigation might be as follows.

The starting point would be to solve (33)–(39) (with ϵ set to zero) for ψ and C, right out to the edge of the cylinder $r = r_0$. The small-r expansion of §5.1 will not suffice and, by analogy with the paradigm, we should expect Γ to vary by an $O(1)$ amount across the cylinder. From the analysis of §5.1 we know that there will be a one-parameter family of solutions to this problem and our job is to select one member of this family. The next step would be to perform a local analysis near $r = r_0$. It is clear that our infinite-gravity limit breaks down in a neighbourhood of the rim, the water flowing over the rim at an elevation determined by a balance between inertia and gravity. However one can, at least formally, take the limit of zero Froude number, in which the free surface is flat right up to a line sink at $r = r_0$. This simplification is justified by the lack of dependence of the experimental measurements on the details of the flow over the edge. Now, since the Reynolds number (and thus also the Péclet number) is large even based on the pump velocity U_p, the boundary layer structure persists right up to the sink, as in Jefferey-Hamel flow (see Ockendon and Ockendon (1995)), and the full Navier-Stokes equations will not have to be solved at any stage.

The asymptotic structure of this region is very much more complicated than for the paradigm equation. If our hypothesis is correct then requiring Γ to be regular as $r \to r_0$ should pick out a particular local solution. Thus we should be able to select one member of the family of zero-ϵ (numerical) solutions obtained in $r < r_0$ which has the correct behaviour near $r = r_0$.

6 Conclusion and Discussion

We have presented a theory which explains the ability of a weak bulk concentration of surfactant to enhance surface expansion in the overflowing cylinder experiment, as observed by Manning-Benson *et al.* (1997, 1998a,b). The insight that this theory offers is that the diffusive flux of surfactant towards the free surface is, in steady flow, balanced by a convecting boundary layer in which the typical dilatation rate is given by (10). Thus the dramatic increase in surface velocity brought about by the presence of the surfactant should be thought of in terms of diffusion rather than surface tension gradients; the latter are set up by the former.

It is unfortunate that, in the absence of a substantial numerical investigation, we have been unable to close our theory. Our conjecture is that the diffusive nature of the spread of surfactant in the surface, which is quite different from so-called "surface diffusion", determines not only the order of magnitude of

the surface velocity, but also its precise value, because of the information that diffusion transmits from the rim of the cylinder.

The variation in surface velocity given theoretically by (50) agrees well with the observed values if the bulk concentration is sufficiently high. The experimental evidence points to a link between the discrepancy at low bulk concentrations and the corresponding lower-than-expected measurements of surface concentration. These presumably arise from unusually slow transfer of surfactant molecules from the bulk into the surface, for which electrical double layer effects have been proposed as a mechanism. Incorporation of such effects into our model may help to verify whether they do explain the apparently anomalous behaviour.

The delicacy of the calculations leading to the predictions of Figure 8 highlight the need for more experiments to be done, especially at low concentrations. It would also be helpful for experiments to be performed using non-ionic surfactants to eliminate any electrostatic influence.

We emphasise again the experimental evidence that neither the size of the cylinder nor the shape of the rim appears to influence the flow near the axis significantly. The solution procedure proposed at the end of §5 takes advantage of these observations by considering the behaviour near the rim in isolation. The resulting local flow, namely that of a surfactant-loaded free surface into a sink at high Reynolds number, strikes us as a fundamental problem in fluid mechanics, an interesting generalisation of the classical Jefferey-Hamel flow and a challenging exercise in asymptotic analysis.

Acknowledgements

The authors are very grateful for the assistance and advice of Dr C. D. Bain and Dr S. Manning-Benson, and for many helpful discussions with Dr S. D. Howison and Prof. J. F. Harper. Part of this work was carried out with the financial support of an EPSRC studentship (CJWB) and a Junior Research Fellowship from Christ Church, Oxford (PDH).

References

Adamson, A.W. (1982). *Physical chemistry of surfaces, 4th Ed.* J Wiley and Sons.

Bain, C.D., Manning-Benson, S., Darton, R.C. (2000). Rates of mass transfer

and adsorption of Hexadecyltrimethylammonium Bromide at an expanding air-water interface. *J. Coll. Int. Sci.*, 229, 247—286.

Bergink-Martens, D.J.M., Bos, H.J., & Prins, A. (1994). Surface dilation and fluid-dynamical behaviour of Newtonian liquids in an overflowing cylinder. ii. surfactant solutions. *J. Coll. Int. Sci.*, 165, 221–228.

Bergink-Martens, D.J.M., Bos, H.J., Prins, A., & Schulte, B.C. (1990). Surface dilation and fluid-dynamical behaviour of Newtonian liquids in an overflowing cylinder. i. pure liquids. *J. Coll. Int. Sci.*, 138, 1–9.

Bergink-Martens, D.J.M., Bos, H.J., Prins, A., & Zuidberg, A.F. (1992). Surface dilational behaviour of surfactant solutions. *Coll. Surf.*, 65, 191–199.

Grunnet-Jepsen, H., Darton, R.C., & Whalley, P.B. (1995). Modelling foaming behaviour. In R. Agrawal and L. Dall-Bauman, editors, *Recent Developments and future opportunities in separations technology.* AIChE annual meeting at Miami Beach, AIChE. Paper 19b.

Jensen, O.E., and Halpern, D. (1998). The stress singularity in surfactant-driven thin-film flows. part 1. viscous effects. *J. Fluid Mech.*, 372, 273–300.

Manning-Benson, S. (1998). *The dynamics of surfactant adsorption.* PhD thesis, University of Oxford, 1998.

Manning-Benson, S., Bain, C.D., & Darton, R.C. (1997). Measurement of dynamic interfacial properties in an overflowing cylinder by ellipsometry. *J. Coll. Int. Sci.*, 189, 109–116.

Manning-Benson, S., Bain, C.D., Darton, R.C., Sharpe, D., Eastoe, J., & Reynolds, P. (1997) Invasive and non-invasive measurements of dynamic surface tensions. *Langmuir*, 13, 5808–5810.

Manning-Benson, S., Parker, S.W.R., Bain, C.D., & Penfold, J. (1998). Measurement of the dynamic surface excess in an overflowing cylinder by neutron reflection. *Langmuir*, 14, 990–996.

Ockendon, H., & Ockendon, J.R. (1995) *Viscous Flow.* Cambridge University Press.

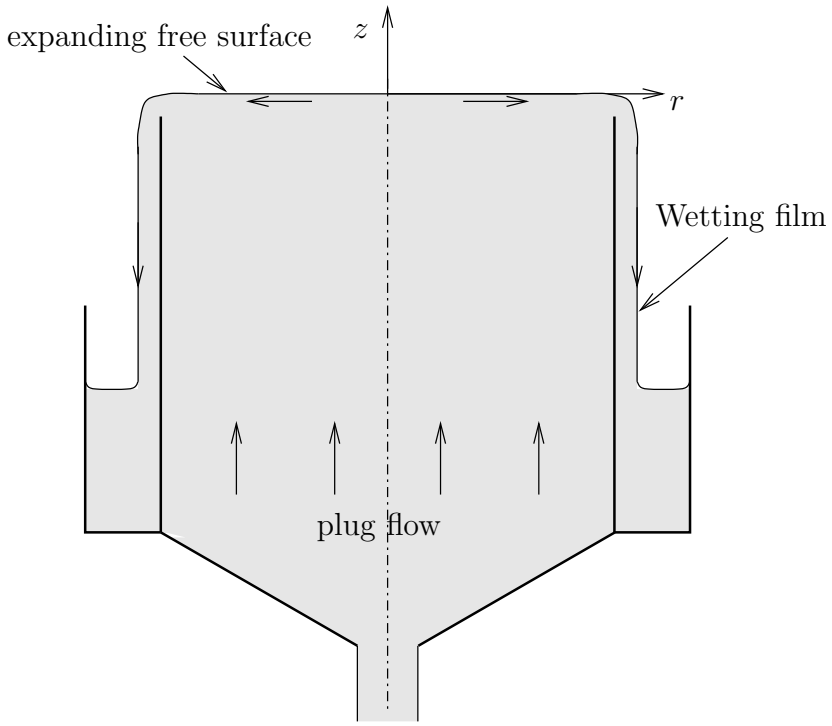

Fig. 1. Schematic of the overflowing cylinder apparatus.

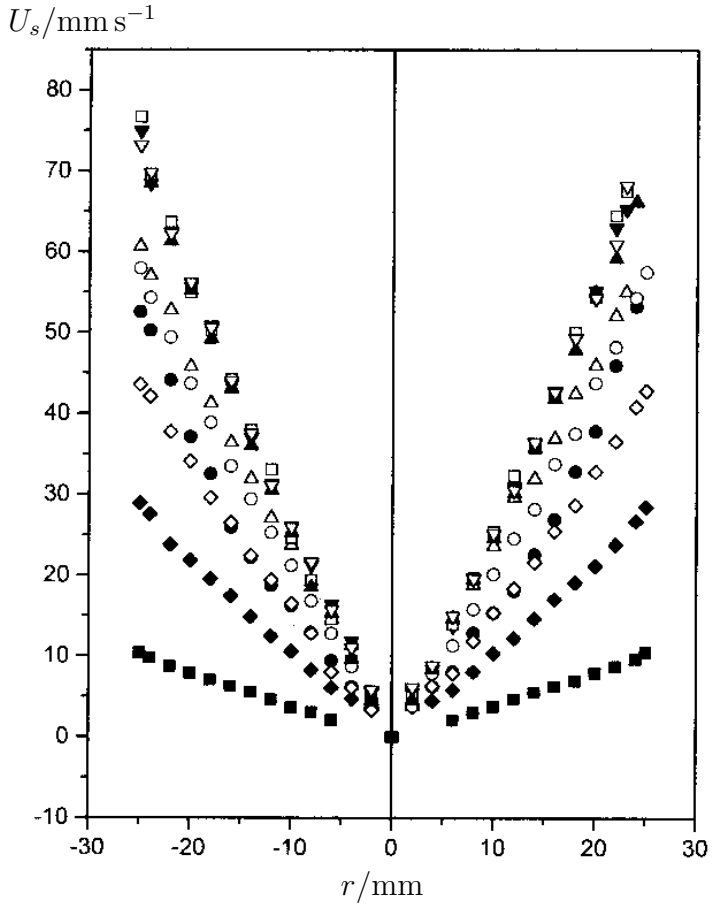

Fig. 2. Radial surface speed as a function of distance r from the origin, for bulk concentrations $0.1\,\mathrm{mol\,m^{-3}}$ (■), $0.25\,\mathrm{mol\,m^{-3}}$ (♦), $0.35\,\mathrm{mol\,m^{-3}}$ (◊), $0.46\,\mathrm{mol\,m^{-3}}$ (○), $0.58\,\mathrm{mol\,m^{-3}}$ (▲), $0.68\,\mathrm{mol\,m^{-3}}$ (▽), $0.81\,\mathrm{mol\,m^{-3}}$ (□). (We ignore the other measurements which are above the critical micelle concentration.)

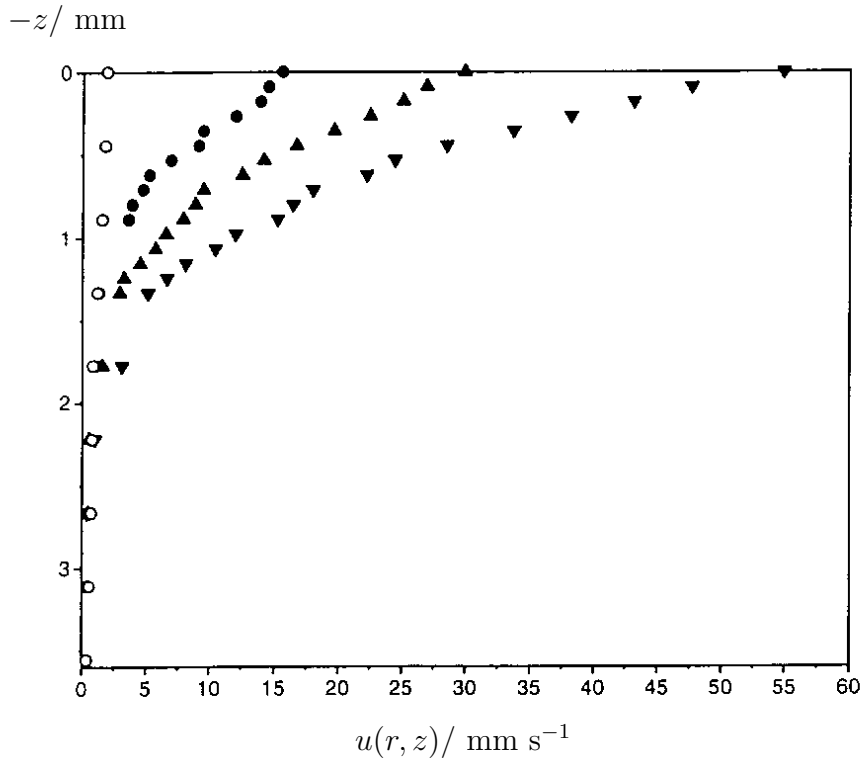

Fig. 3. Subsurface velocity profiles versus depth, $-z$, at $r = 6\,\mathrm{mm}$ (•), $r = 12\,\mathrm{mm}$ (▲) and $r = 20\,\mathrm{mm}$ (▼), for bulk concentration $0.58\,\mathrm{mol\,m^{-3}}$.

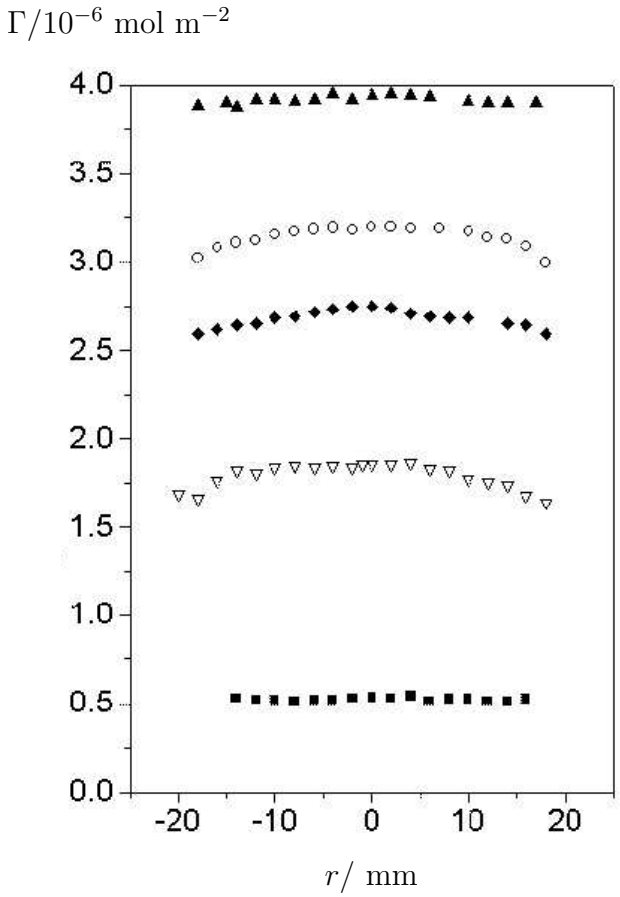

Fig. 4. Surface concentration of surfactant, for bulk concentrations $0.1\,\mathrm{mol\,m^{-3}}$ (■), $0.31\,\mathrm{mol\,m^{-3}}$ (▽), $0.58\,\mathrm{mol\,m^{-3}}$ (♦), $0.81\,\mathrm{mol\,m^{-3}}$ (○) and $1.73\,\mathrm{mol\,m^{-3}}$ (▲).

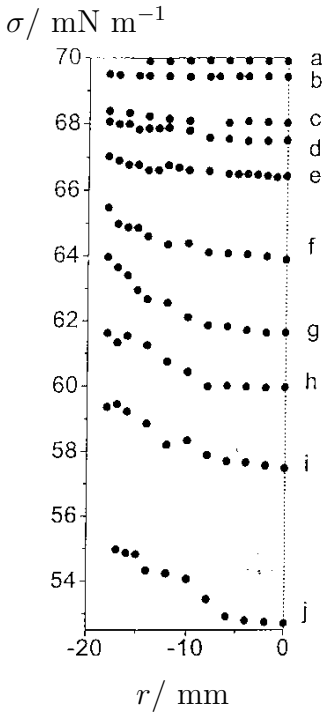

Fig. 5. Surface tension variations for bulk concentrations of (a) 0.1, (b) 0.17, (c) 0.25, (d) 0.31, (e) 0.35, (f) 0.46, (g) 0.51, (h) 0.58, (i) 0.68, (j) 0.81 mol m^{-3}.

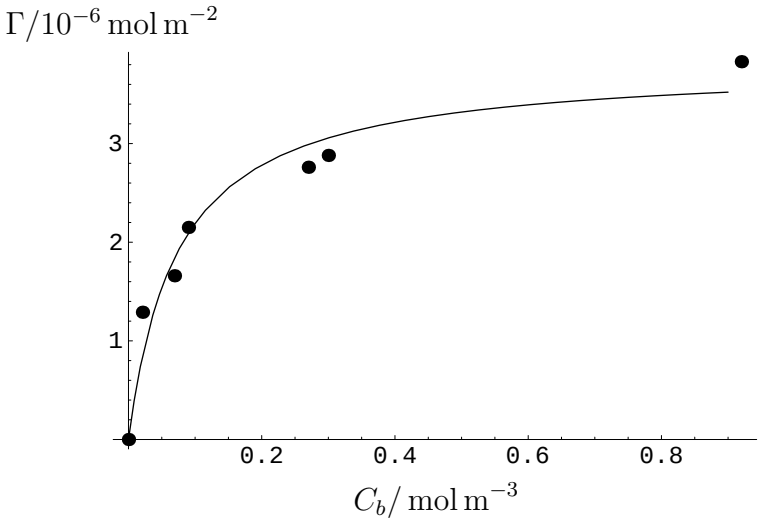

Fig. 6. Experimental static values of surface concentration Γ and subsurface bulk concentration C_s, fitted with a Langmuir isotherm $\Gamma = \Gamma_{\rm sat} C_s/(k + C_s)$. The least-squares fit has parameter values $\Gamma_{\rm sat} = 3.81 \times 10^{-6}\,{\rm mol\,m^{-2}}$, $k = 0.074\,{\rm mol\,m^{-3}}$.

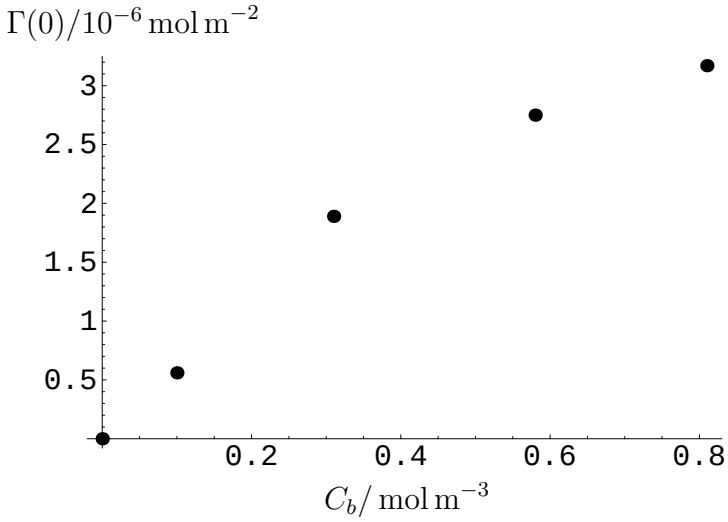

Fig. 7. Experimentally measured values of surface concentration $\Gamma(0)$ versus bulk concentration C_b.

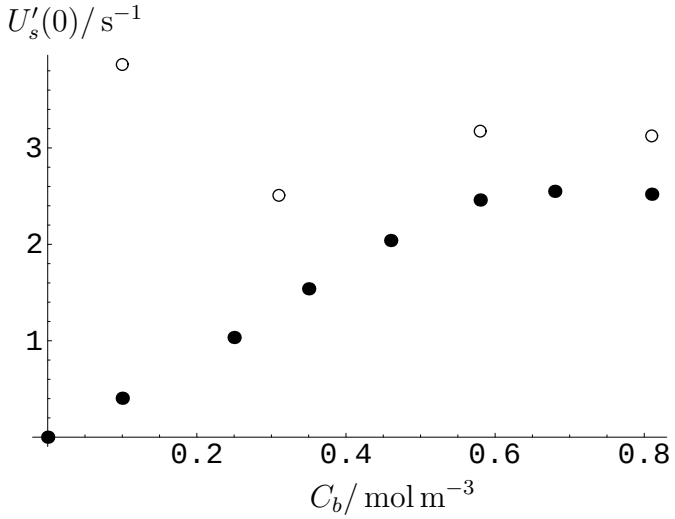

Fig. 8. Dilatation rate $U_s'(0)$ versus bulk concentration C_b. The open circles are theoretical predictions, obtained using (50), (51) and Figure 7. The filled circles are experimental values.